*35th EPS Conference on Plasma Phys. Hersonissos, 9 - 13 June 2008 ECA Vol.**32D**, P-2.085 (2008)*

# EMC3/EIRENE Transport Modelling of the Island Divertor in W7-X

Y. Feng, J. Kisslinger, F. Sardei, D. Reiter[§]

*Max-Planck-Institut fuer Plasmaphysik, Euratom Association, Greifswald/Garching*
*[§]Institut fuer Energieforschung-Plasmaphysik, Forschungszentrum Juelich GmbH, Euratom Association, Trilateral Euregio Cluster, D-52425 Juelich, Germany*

## 1. Introduction

W7-X will be equipped with ten divertor modules [1] of the same type as the island divertor (ID) tested on W7-AS [2]. Island divertor transport in W7-AS has been studied extensively. Good agreement in global physics is found between simulations and experiments [3]. On the basis of the numerical and experimental results gathered from W7-AS, a detailed parameter pre-study for the W7-X ID has been planned, covering an appropriate range of configurations and uncertainties in transport and plasma-surface interaction. The work has begun with estimating the neutral particle compression and exhaust capability of the W7-X divertor [4] and assessing the possible effects of β-induced ergodicity on plasma transport [5]. The work presented in this paper addresses transport essentials of plasma, neutrals and impurities associated with the specific ID geometry in W7-X (see figure 1). In particular, it is focussed on a comparison of divertor transport between two devices having the same divertor concept but different size.

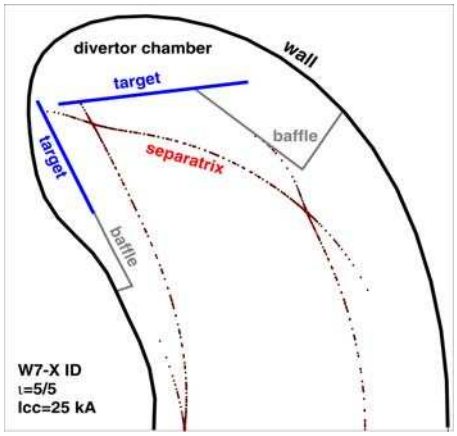


Fig. 1: The W7-X island divertor.

## 2. Geometrical comparison between W7-AS and W7-X

W7-X differs from W7-AS not only in the increased machine size but also in the up-shifted operational ι-window in which the ι=5/6, 5/5, 5/4 island chains are suitable for the ID, with ι=5/5 being the standard case. The divertor-relevant geometric parameters for W7-AS and W7-X are listed in Table 1, where the last four parameters have only representative meanings because of the complex 3D SOL structures. Taken into account are only the respective standard divertor configurations, with the islands being maximally enlarged by control coils installed on each device. The importance of the control coils for improving the

Table 1: Comparison of island-divertor-relevant geometric parameters between W7-AS and W7-X.
*$L_c$=target-target connection length, $\Delta x$=target-core distance, $\Delta y$ = poloidal island width, $\Theta$ = pitch*

| | R (m) | a (m) | ι | $L_c$ (m) | Δx(cm) | Δy(cm) | $\Theta$ ($10^{-3}$) |
|---|---|---|---|---|---|---|---|
| W7-AS | 2.0 | 0.14 | 5/9 | ~100 | ~4 | ~10 | ~1-1.5 |
| W7-X | 5.5 | 0.50 | 5/5 | ~180 | ~7-8 | ~ 60 | ~2-3 |

island divertor performance has been demonstrated in W7-AS [6]. Since the radial island size scales as $r_i \propto \sqrt{Rb_{mn}/n\iota'}$ ($R$ = major radius, $b_{mn}$ = normalized resonant radial perturbation field, $n$ = poloidal mode number, $\iota'$ = the shear), both the larger $R$ and the smaller $n$ in W7-X increase $r_i$, providing a wider target-core-separation $\Delta x$. Bigger islands have also larger connection lengths $L_c$ since $L_c = 2\pi R/nr_i\iota' \propto r_i/b_{mn}$ [3]. The field line pitch $\Theta$ given in Table 1 is determined for the divertor region by measuring the X-point-to-target connection length $L_{c,x\text{-}t}$, i.e. $\Theta = \Delta x/ L_{c,x\text{-}t}$. The average pitch $\Theta = r_i\iota' a/R$ ($a$ = minor radius) [3] is even larger due to the poloidal elongation of the W7-X islands. For linearly scaled devices, however, $\Theta$ will remain unchanged while $r_i$ and $L_c$ linearly scale with the machine size.

## 2. 3D simulation results

*High Recycling regime predicted for W7-X.* The larger field line pitch in W7-X decreases the perpendicular-to-parallel transport ratio, generally reducing perpendicular viscous transport. Moreover, the large poloidal extension of the W7-X islands avoids cross-field frictional momentum interaction between adjacent island fans. This suggests that the SOL transport in W7-X should behave differently from that in W7-AS. This is indeed shown by EMC3/EIRENE simulations, as demonstrated in figures 2 and 3. Simulations are carried out for pure hydrogen plasmas without impurities. The SOL power for W7-AS is taken to be 1 MW which is up-scaled with the area of the LCFS to 10 MW for W7-X. The cross-field transport coefficients are set as D = 1 $m^2/s$ and $\chi_i=\chi_e$=3D which hold for both devices. At low plasma separatrix density $n_{es}$, both devices show linear growths of the recycling flux $\Gamma_{recy}$ and the downstream density $n_{ed}$ with increasing $n_{es}$ up to ~$1.3\times10^{19}$ $m^{-3}$. Then, the W7-X results suddenly depart from the linear behaviour further followed by W7-AS. In this range, $n_{ed}$ in W7-X approaches a scaling of $n_{ed} \sim n_{es}^3$ and greatly exceeds $n_{es}$, as it usually behaves in a high recycling regime found in tokamaks. W7-X is the first helical device for which a high recycling regime is predicted not only by the 3D code but also by 2D approximations [7]

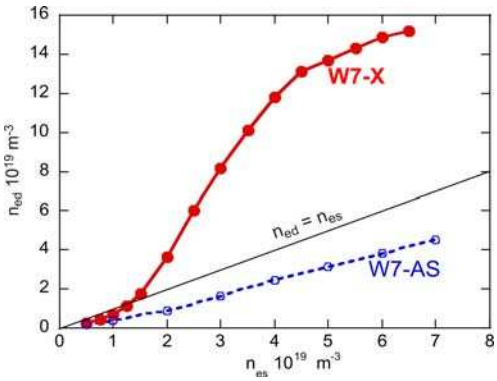


Fig.2: Comparison of $n_{es}$-dependences of the downstream density $n_{ed}$ between W7-AS and W7-X.

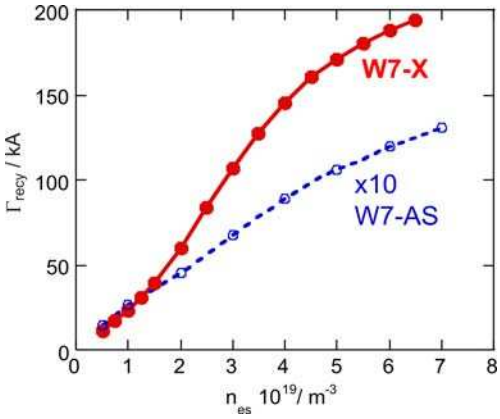


Fig.3: Responses of the total recycling flux $\Gamma_{recy}$ to the spepatrix density $n_{es}$ predicted for the respective W7-AS and W7-X standard island divertors.

*Impurity retention.* The island screening potential of intrinsic impurities, as predicted for W7-AS and LHD [8, 9], is also examined for the W7-X ID. Using the calculated background plasmas shown in figures 1 and 2, test carbon impurities are started from the targets with mono-energies of $E_0$ = 0.1, 1 and 10 eV, respectively, covering both chemical and physical sputtering processes. A lower $n_{es}$–boundary is set at $1\times10^{19}$ $m^{-3}$ to cut off the low SOL collisionality cases where $\lambda_{i,e}/L_c < 10$. All the $E_0$-cases show sharp drops of $n_{cs}$ in the $n_{es}$-range from 1 to $2\times10^{19}$ $m^{-3}$. This is associated with a transition from thermal-force to friction-dominated impurity transport. In comparison with W7-AS, the transition in W7-X is sharper and shifted to lower $n_{es}$ because of the high recycling regime. Higher-energetic carbon neutrals penetrate more deeply into the SOL, causing an overall increase in $n_{cs}$. Nevertheless, their $n_{es}$-dependences are largely insensitive to $E_0$, meaning that the SOL density is always a sensitive tuning parameter for controlling the influxes of both the chemically and physically sputtered impurities.

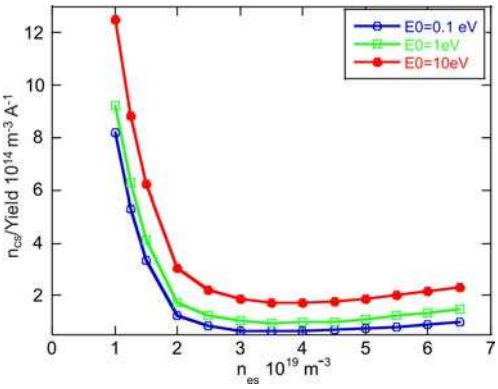


Fig. 4: Sensitivities of carbon density at the inner separatrix, $n_{cs}$, to $n_{es}$ and initial energy of the sputtered carbon atoms, $E_0$. $n_{cs}$ is normalized to a total carbon production rate of $1/1.6\times10^{-19}$ $s^{-1}$.

*Detachment.* The W7-X calculations shown in figures 2 and 3 have been repeated by adding the target-released carbon impurities. The sputtering coefficient is fixed to be 2%. Figure 5 shows a drastic change in carbon radiation at $n_{es} \sim 3\times10^{19}$ $m^{-3}$, indicating the transition to detachment. This is also reflected by the sudden drops in $\Gamma_{recy}$ and $n_{ed}$ shown in figure 6. The maximum $n_{ed}$ reached at rollover is by more than factor 3 higher than $n_{es}$. Note that $n_{ed}$ is always smaller than $n_{es}$ in W7-AS, even at rollover point. The existence of a prior high recycling regime in W7-X allows an earlier onset of detachment in $n_{es}$-space.

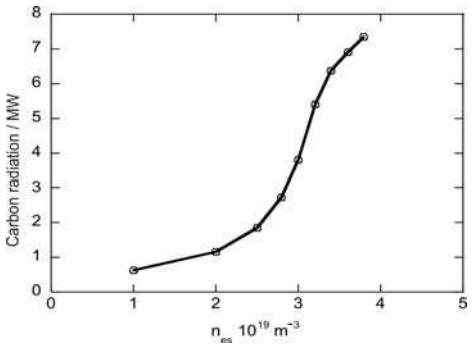


Fig. 5: Carbon radiation as a

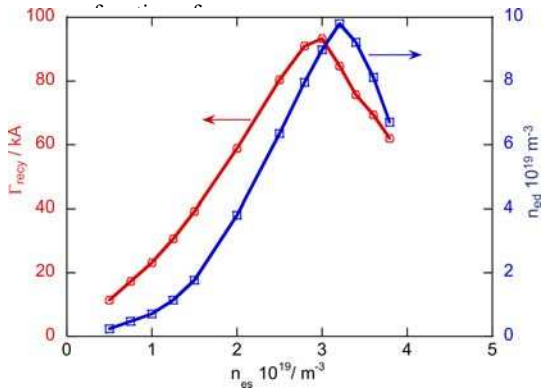


Fig. 6: Developments of $\Gamma_{rec}$ and $n_{ed}$ with increasing $n_{es}$.

*Neutral screening.* For measuring core ionization, we define core plasmas by filling the region enclosed by a flux surface ~2 cm inside the LCFS with hydrogen plasmas of constant temperature and density. $T_{core}$ ($T_{core} \equiv T_e = T_i$) is varied to cover uncertainties in core profiles, while the density is fixed to be $1\times10^{20}$ $m^{-}$

$^3$ as the density, for an optically-thick core plasma, is not a sensitive parameter in this study. The three curves shown in figure 7 are different in level but similar in form. The relative levels reflect the $T_{core}$-dependence of the ionization-to-CX ratio in the core. The curve form is determined by the recycling neutral influx, thus reflecting the neutral screening efficiency of the edge islands and the recycling process. The maxima reached at $n_{es} \sim 1\times10^{19}$ are compromise results between two competing effects, i.e. the increasing $\Gamma_{recy}$ and the gradually-improved neutral screening efficiency with raising $n_{es}$. $S_{core}$ drops when the latter effect dominates. Similar behaviour is also predicted for W7-AS. Nevertheless, the drop of $S_{core}$ in W7-X is much stronger than that in W7-AS. Ignoring the detachment regime and combining the impurity screening effects shown in figure 4, we find that there exists a narrow $n_{es}$-window for attached plasmas within which the island divertor exhibits its optimum functionality in terms of recycling, neutral screening and impurity production and shielding. In this window, $S_{core}$ has a negative $n_{es}$-dependence. W7-AS experiments have indicated that the divertor plasmas controlled via gas-puffing using $\overline{n}_e$ as feedback cannot reach steady state in the $n_{es}$-region where $S_{core}$ drops. This suggests that different density control strategies should be considered for W7-X in order to identify stable accesses to the above-mentioned narrow $n_{es}$-window for 'optimum' divertor performance. Furthermore, the improved divertor neutral screening and the expected higher core temperatures (more precisely, the temperatures in the neutral penetration region) in W7-X significantly reduce the recycling-neutral refuelling capability, implying the need for additional particle fuelling sources like NBI and pellets for achieving high density plasmas in W7-X.

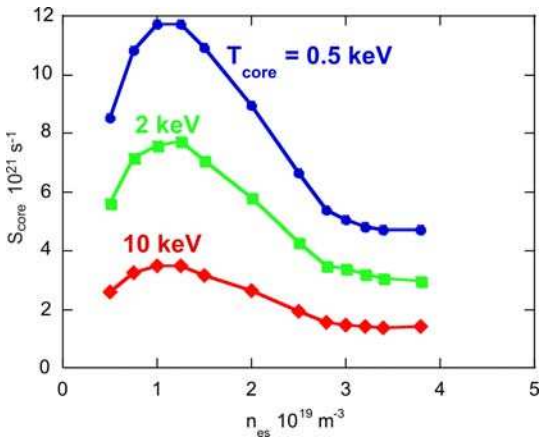


Fig. 7: Dependences of intrinsic particle core refuelling rates on core temperatures and $n_{es}$.

## References

[1] H. Renner et al. Nucl. Fusion 40 (2000) 1083

[2] P. Grigull et al. Plasma Phys. Control. Fusion 43 (2001) A175

[3] Y. Feng et al. Nucl. Fusion 46 (2006) 807

[4] D. Sharma et al. Nucl. Fusion 45 (2005) 825

[5] D. Sharma et al. Nucl. Fusion 46 (2006) S127

[6] P. Grigull et al. J. Nucl. Mater. (2003) 313-316 1287

[7] J. Kisslinger et al. 22nd EPS, Bournemouth, 1995, 19C, III, 149

[8] Y. Feng et al. 32nd EPS, Tarragona ,2005, vol 29 29C (ECA) P1.012

[9] M . Kobayashi et al. PSI 2008